Title	Admittance of a one-dimensional double-barrier resonant tunneling nanostructure
Author(s)	Shangguan, Wang Zuo; Au Yeung, Tin Cheung; Yu, Ya Bin; Kam, Chan Hin; Zhao, Xuean
Citation	Shangguan, W. Z., Au Yeung, T. C., Yu, Y. B., Kam, C. H., & Zhao, X. (2002). Admittance of a one-dimensional double-barrier resonant tunneling nanostructure. Physical Review B - Condensed Matter and Materials Physics, 65(23), 235315-.
Date	2002
URL	http://hdl.handle.net/10220/44724
Rights	© 2002 American Physical Society (APS). This paper was published in Physical Review B - Condensed Matter and Materials Physics and is made available as an electronic reprint (preprint) with permission of American Physical Society (APS). The published version is available at: [doi:http://dx.doi.org/10.1103/PhysRevB.65.235315]. One print or electronic copy may be made for personal use only. Systematic or multiple reproduction, distribution to multiple locations via electronic or other means, duplication of any material in this paper for a fee or for commercial purposes, or modification of the content of the paper is prohibited and is subject to penalties under law.

Admittance of a one-dimensional double-barrier resonant tunneling nanostructure

W. Z. Shangguan, T. C. Au Yeung, Y. B. Yu, and C. H. Kam
School of Electrical and Electronic Engineering, Nanyang Technological University, Singapore 639798

Xuean Zhao
Zhejiang Institute of Modern Physics, Zhejiang University, Hangzhou 310027, China

(Received 12 September 2001; revised manuscript received 4 December 2001; published 29 May 2002)

We study the dynamic response of a one-dimensional double-barrier nanostructure to an ac bias. Combining the Schrödinger equation, Poisson equation and the scattering theory, we calculate the internal potential, charge density, and the ac conductance as well. The results show that the charge distribution is antisymmetric with respect to the center of the double barrier, and depends crucially on the relative position of the Fermi level to the resonant energies of the well. The diagonal emittance is found to have a similar dependence. It is negative (inductive behavior) when the Fermi energy is very close to the resonant energies, and it reaches the negative maximum at resonant energies, while it is always positive (capacitive behavior) when the Fermi energy is within the barrier depth and far from resonance, and develops two peaks closely on both sides of the inductive peak. This result is in agreement with that obtained from discrete model. In addition, we find that the capacitive peaks correspond to the maxima of charge-density fluctuation, and inductive peaks to zero charge-density distribution. Therefore, the sign and magnitude of emittance reflect how the charge piles up inside the device.

DOI: 10.1103/PhysRevB.65.235315 PACS number(s): 72.10.−d

I. INTRODUCTION

Double-barrier resonant tunneling nanostructures (DBRTNS) have attracted great research interest because of their many potential device applications, and their significance in the study of the physics of confined structures. Both dc and ac transport characteristics of the system have been studied extensively while most of the dc transport properties, such as the linear and nonlinear response, as well as the Kondo effect, have been made clear. The current research interest focuses on the ac transport properties, some of these studies are based on simulation of a realistic device using detailed numerical procedures,[1,2] while others are based on simple discrete models.[3–15] However, the effect of time-varying charge density on the systems is still a less-investigated problem, which is important in determining the ac conductance.[2,3,15,16] While Ref. 17 discussed the pitfalls of many existing ac conductance theories qualitatively, Büttiker and co-workers[15,16,18–21] have formulated a theory of ac conductance in the linear response and low-frequency regime that is applicable to mesoscopic structures with charging effects, based on both continuous and discrete models. The effect of time-dependent charge density in and outside the well around the barriers is of importance in determining the dynamic conductance, because charge density and related internal potential will be directly related to the charge and current conservation, as well as the gauge invariance of conductance under an overall potential shift. Recently, with the help of the discrete models including some geometry capacitances, some authors have studied ac conductance and charging effect of the DBRTS, as well as ac Kondo effect.[14,22]

By making use of the continuous model we study in this paper the electronic properties of a DBRTNS such as induced internal potential and charge-density distribution, and low-frequency conductance, to illustrate the role of the induced internal potential and charge density and the influence of reservoir temperature on the ac transport of nanostructure systems, extending the discussions in Ref. 23. As the DBRTNS is a typical resonant device, we study its electronic transport properties around and far from resonance, and explore the difference between them. Our particular interest focuses on the effect of temperature on these transport properties.

Our calculation of the internal potential and charge density shows that when the transmission probability is small (far from resonance), the antisymmetrical charge distribution exists only around the double barrier under the influence of the applied ac voltage. For the case of near resonance with a large transmission probability (but $|s_{12}|^2<1$), we find a considerable amount of charge pile up in the well region as well as on both sides beyond the double barrier. As for resonant case or when the incident energy of the carriers is much higher than the barrier height, our results show that the charge distribution around the double barrier is almost zero. We find that the diagonal emittance (low-frequency term of ac conductance) depends crucially on the relative energy of the Fermi level to the resonant energies. It is negative (reflecting inductive behavior) when the Fermi energy is very close to the resonant energies but within the barrier height, and reaches the negative maximum (inductive peak) at resonant energies, while it is always positive (reflecting capacitive behavior) and develops two positive maxima (capacitive peaks) near but on the both sides of the inductive peak when the Fermi energy is far from resonant energy. This result is in agreement with that in Ref. 15. In addition, we find that the capacitive peaks correspond to the maxima of charge-density fluctuation, and inductive peaks to zero charge-density distribution. Therefore, the sign and magnitude of the emittance reflect how the carriers pile up in the system under the application of an ac field, and how the temperature of the system affects the carrier pileup and in turn affects the distribu-

tion of the internal potential and the admittance. This is in accordance with the previous works by Büttiker and co-workers.[24]

II. THEORY

The local partial density of states (LPDOS) is a very important concept in the scattering theory of quantum transport in mesoscopic conductors.[19] It originates from the displacement current that is the response of the long-range coulomb interaction to an ac perturbation in electron reservoirs. The LPDOS is given by

$$\frac{dn_{\alpha\beta}(x)}{dE}=\frac{-1}{4\pi i}\int dE\left(\frac{-\partial f}{\partial E}\right)\left[s^{\dagger}_{\alpha\beta}\frac{\delta s_{\alpha\beta}}{\delta U(x)}-\frac{\delta s^{\dagger}_{\alpha\beta}}{\delta U(x)}s_{\alpha\beta}\right], \tag{1}$$

where α, β are the leads indices, and $s_{\alpha\beta}$ are the elements of the scattering matrix. We consider in this paper the tunneling model of a one-dimensional double-barrier potential connected to two leads with a finite cross-sectional area, which is assumed to be a constant. However, here we study only the case in which the Fermi levels in the left and right reservoir are equal so that the internal potential is due solely to the ac perturbation in the electron reservoirs.

For a general one-dimensional scattering potential, the scattering matrix can be determined by partitioning the one-dimensional space into many narrow regions and using the transfer matrices between two neighboring regions. The transfer matrix between two neighboring regions is obtained by matching the wave functions and their derivatives at the boundary of the two regions. With the LPDOS defined in Eq. (1) the injectivity can be defined by

$$\frac{dn_{\alpha}(x)}{dE}=\sum_{\beta}\frac{dn_{\alpha\beta}(x)}{dE}, \tag{2}$$

which describes the carrier density of states incident in the probe α regardless of which probe it goes out.[16] This is justified by the formula of $dn_{\alpha}(x)/dE$ derived by Gasperian *et al.*[20]

$$\frac{dn_{\alpha}(x)}{dE}=\int dE\left(\frac{-\partial f}{\partial E}\right)\frac{1}{hv_{\alpha}}|\psi_{\alpha}(x)|^2, \tag{3}$$

where v_{α} is the incident velocity of the carriers and $\psi_{\alpha}(x)$ is the scattering wave function.

In the presence of a small ac voltage v_{ac} applied to the probe α ($\alpha=1,2$), the internal potential $U(x)$ is given by $U(x)=u_{\alpha}(x)ev_{ac}$, where u_{α} is termed characteristic function. The internal potential is caused by the charge distribution around the mesoscopic conductor under an ac voltage. Using the Thomas-Fermi approximation, the characteristic function u_{α} satisfies the Poisson equation:[16,21]

$$-\nabla^2 u_{\alpha}+\frac{e^2}{\varepsilon_0}\frac{dn(x)}{dE}u_{\alpha}(x)=\frac{e^2}{\varepsilon_0}\frac{dn_{\alpha}(x)}{dE}\quad(\alpha=1,2), \tag{4}$$

where $dn(x)/dE=dn_1(x)/dE+dn_2(x)/dE$ is the total local density of states. Under the Thomas-Fermi approximation the second term in Eq. (4) is the induced charges in the conductor and the third term is clearly the injected charges. For finite cross-sectional area of the leads, we should have the transverse direction (y and z), and the formula (4) for the injectivity should be multiplied by $|\phi(y,z)|^2$, where $\phi(y,z)$ is the wave function describing the confinement of the carriers in the transverse direction. If we assume that u_{α} depends on x only, we obtain the following equation by integrating over y and z and using the fact that $\int dydz|\phi(y,z)|^2=1$:

$$-\frac{d^2u_{\alpha}(x)}{dx^2}+\frac{e^2}{\varepsilon_0 A}\frac{dn(x)}{dE}u_{\alpha}(x)=\frac{e^2}{\varepsilon_0 A}\frac{dn_{\alpha}(x)}{dE}, \tag{4a}$$

where A is the finite cross-sectional area of the left and right leads. It is noticed that the case of infinite cross-sectional area has been considered by Zhao *et al.*[23]

To solve Eq. (4a) for $u_{\alpha}(x)$, we need the boundary values of $u_{\alpha}(x)$. In Ref. 23 the authors used the neutrality condition to determine the boundary values of $u_{\alpha}(x)$:

$$u_1(x_L)=\frac{dn_1(x_L)}{dE}\Big/\frac{dn(x_L)}{dE},$$

$$u_1(x_R)=\frac{dn_1(x_R)}{dE}\Big/\frac{dn(x_R)}{dE},$$

$$u_2(x_L)=u_1(x_R),\qquad u_2(x_R)=u_1(x_L), \tag{5}$$

However, the authors only considered the zero-temperature case ($T=0$) where the injectivity is much simple to calculate

$$\frac{dn_{\alpha}(\mathrm{x_L})}{dE}=\frac{1}{hv_{\alpha}}|\psi(x)|^2. \tag{3'}$$

Equation (3′) implies immediately that $u_1(x_L)=(1+|s_{11}|^2)/2$ and $u_1(x_R)=(1-|s_{11}|^2)/2$ when $T=0$. Physically, the point x_L (x_R) is located somewhere in the left (right) lead where the charge vanishes. In addition to the zero-temperature case we study in this paper also the nonzero temperature case, which provokes Eq. (3) instead of Eq. (3′). Accordingly, we have

$$u_1(x_L)==\int dE\left(\frac{-\partial f}{\partial E}\right)\frac{1+|s_{11}|^2}{hv}\Big/\int dE\left(\frac{-\partial f}{\partial E}\right)\frac{2}{hv},$$

$$u_1(x_R)==\int dE\left(\frac{-\partial f}{\partial E}\right)\frac{1-|s_{11}|^2}{hv}\Big/\int dE\left(\frac{-\partial f}{\partial E}\right)\frac{2}{hv}. \tag{6}$$

With the quantities of LPDOS, injectivities and internal potentials obtained, one can then proceed to calculate the admittance at low frequencies:[15,19]

$$g_{\alpha\beta}(\omega)=g_{\alpha\beta}(0)-i\omega e^2E_{\alpha\beta}, \tag{7}$$

where ω is the frequency of the ac bias, $g_{\alpha\beta}(0)$ the dc conductance, and

$$E_{\alpha\beta}=\int dE\left(\frac{-\partial f}{\partial E}\right)\int dx\left[\frac{dn_{\alpha\beta}(x)}{dE}-\frac{dn_{\alpha}(x)}{dE}u_{\beta}(x)\right] \tag{8}$$

is the emittance. The term $\int dx dn_{\alpha\beta}(x)/dE$ is interpreted as the global carrier density of states for those carriers injected into lead β and going out lead α. Thus the first term in Eq. (10) multiplied by $e^2 v_{ac}$, where v_{ac} is a small ac bias applied to probe β, gives the injected charges for those carriers injected into lead β and going out lead α. On the other hand, the second term in Eq. (8) multiplied by $e^2 v_{ac}$ represents the corresponding induced carrier density based on the Thomas-Fermi model. Therefore, we conclude that the quantity $e^2 E_{\alpha\beta} v_{ac}$ is equal to the net charge in the conductor caused by those carriers injected into lead β (by v_{ac}) and going out lead α. The charge $e^2 E_{\alpha\beta} v_{ac}$ will be scattered to the contact α. It is interpreted as the displacement charge.[24] When E_{11} is positive, $e^2 E_{11}$ behaves like an effective capacitance. And we have inductive behavior for the conductor when E_{11} is negative.[24]

For the convenience of numerical computation, we use the double-barrier height V_0 as units of energy and the corresponding wave length λ $(=2\pi/\sqrt{2mV_0/\hbar^2})$ as units of length. Hence we shall set the double barrier $V_0(x)$ to be of unit height in the numerical computation for the scattering wave functions and the scattering matrices. We denote the barrier width and well width by a and $2b$, respectively. Therefore in these new units of energy and length, the Poisson equation (4a) reads

$$-\frac{d^2 u_\alpha(x)}{dx^2} + \sigma \frac{dn(x)}{dE} u_\alpha(x) = \sigma \frac{dn_\alpha(x)}{dE}, \qquad (4')$$

where the parameter $\sigma = e^2 h/(\sqrt{2m}\varepsilon_0 A (V_0)^{3/2})$. It is clear that the parameter σ has considerable effect on the internal potential. The expression of σ here tells us that it is inversely proportional to the cross-sectional area of the leads A and has a nonlinear dependence on the barrier height V_0.

III. NUMERICAL RESULTS AND DISCUSSION

We study the internal potential $u(x)$ with various Fermi levels μ $(=\mu_L=\mu_R)$ and temperatures T. As aforementioned we use V_0, the height of the double barrier $V_0(x)$, as units of energy and $\lambda = 2\pi/\sqrt{2mV_0/\hbar^2}$ as units of distance. Here we consider several cases of barrier width a and well width $2b$. From Eq. (4′), we know that the number density of electrons or charge-density distribution is given by

$$n(x) = -\frac{1}{\sigma}\frac{d^2 u}{dx^2}(x), \qquad (9)$$

where $\sigma = e^2 h/\sqrt{2m}\varepsilon_0 A (V_0)^{3/2}$. As an example, we set $A = 100$ nm^2 (the cross-section area of the left and right leads) and $V_0 = 100$ meV, which means that $\sigma = 7.02$. With this value of σ, we numerically solve the Poisson equation (4′) for $u(x)$, and Eq. (9) for $n(x)$. As for the points of neutrality (x_L and x_R), we set $x_L = -4$ and $x_R = 4$.

In Fig. 1 we plot $|s_{21}|^2$ against the incident energy E for $a=1$ and $b=2$. In the region $E<1$, one can find eight very sharp peaks with unit height. These peaks correspond to the resonant states, which indicate eight quasibound states in the quantum well and which are related to the bound states of the isolated well. For $E>1$, $|s_{21}|^2$ approaches 1 asymptotically and wavily.

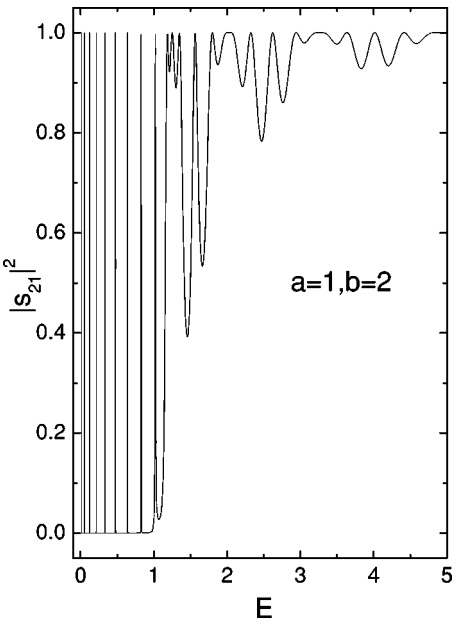

FIG. 1. Plots of transmission probability $|s_{21}|^2$ against the incident energy of charge carriers.

In Fig. 2 we present plots of $u(x)$ and $n(x)$ at $T=0$, for various Fermi energies μ. Figure 2(a) corresponds to the case of $a=1$, $b=2$, and $\mu=0.1$. In this case, the incident energy $\mu=0.7$ is far from resonance. We see that $u(x) = 1(0)$ on the left (right) side of the double barrier, and the shape of $u(x)$ is almost a straight line inside the double barrier. This indicates that the charge distribution $n(x)$ is nonzero only around the left and right barriers, as is shown by the curve (solid line). It is noticed that the charge distribution is antisymmetric with respect to the center of the double barrier $(x=0)$. This implies that the charges accumulated around the left and right barriers are equal in magnitude but opposite in sign.

The parameters for Fig. 2(a) are $a=1$, $b=2$, $\mu = 0.826\,927$, and $T=0$. The incident energy $\mu = 0.826\,927$ corresponds to a resonant state in the double barrier and the peak of $|s_{21}|^2$ is equal to one (high transmission). The graph of $u(x)$ is confined to 0.5 with very small fluctuations. The value of 0.5 is equal to the boundary values $u(x_L)$ $[=(1+|s_{11}|^2)/2]$ and $u(x_L)$ $[=(1-|s_{11}|^2)/2]$ as $|s_{11}|^2 = 0$ in this case. The charge distribution $n(x)$ is very small (near zero) as indicated by the curve.

We set $a=1$, $b=2$, $\mu=1.5$, and $T=0$ in Fig. 2(c). As the incident energy $\mu=1.5$, the reflection probability $|s_{11}|^2$ drops to 0.5. The curve of $u(x)$ has lots of fluctuations beyond and within the double barrier. The charge distribution is large as shown by the charge-density curve (solid line) in this figure. We note again that the charge distribution is antisymmetric with respect to the center $x=0$. For very large incident energy μ, say, $\mu=5$, which is much higher than the unit barrier height [Fig. 2(d)], the curve of $u(x)$ is strictly a con-

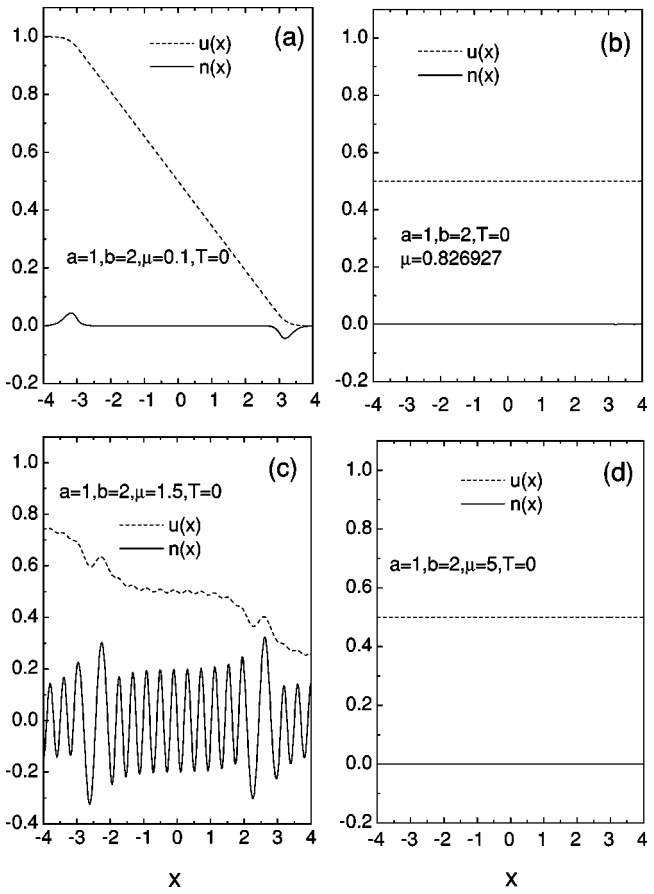

FIG. 2. The distribution of internal potential (dashed line) and charge density (solid line) for $a=1$, $b=2$, and $T=0$. (a) The small-transmission case, $\mu=0.7$, (b) The resonant case, $\mu=0.269\,27$, (c) $\mu=1.5$, above the barriers, and (d) $\mu=5$, well above the barrier height.

stant equal to 0.5 $[=u(x_L)=u(x_R)$ as $|s_{11}|^2=0]$. We conclude that the charge distribution is zero around the double barrier.

Now let us make a comparison of the charge responses among the situations of resonance, near resonance and far from resonance. In Fig. 3, we present the results of the charge response for the different chemical potentials. We start from the resonant case $\mu=0.826\,927$. As μ deviates from the resonant energies the charge-density distribution increases. However, as it deviates further, the charge-density distribution begins to decrease after reaching a maximum, and tends to the case of Fig. 2(a). So there is a maximum charge response between resonant and low transmission cases. Moreover, there are a lot of fluctuations in the curve of $u(x)$ in the case of large charge response, and hence there is a large and antisymmetric charge distribution around the double barrier.

From the above results we can conclude that when the transmission probability $|s_{21}|^2$ is small (nonresonant case), the antisymmetrical charge distribution exists only around the double barrier as a response to the applied ac voltage, and the charges from one side of the conductor is driven to the other side. As the transmission is low, the charges on the other side cannot penetrate through the double barrier that

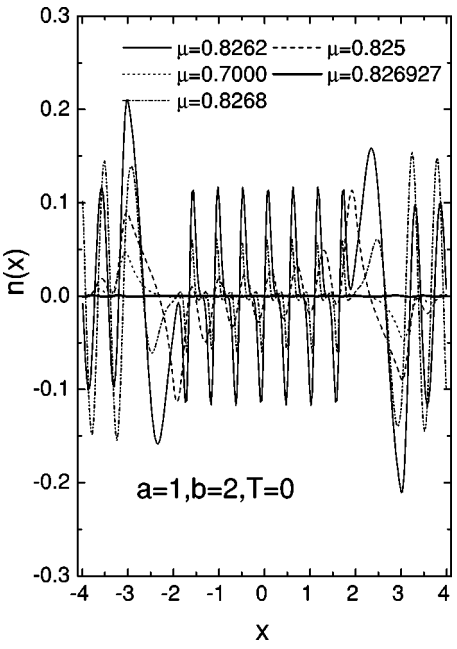

FIG. 3. A comparison of charge-density distribution among different Fermi energies.

leads to an antisymmetric charge distribution around the two barriers. On the other hand, for high transmission (resonant case with large peak, $|s_{21}|^2=1$) or the incident energy much higher than the barrier height, the above results show that the charge distribution around the double barrier is very small. We also expect this because in this case the carriers can penetrate through double barrier easily, thus the charges are driven by the ac voltage through the conductor neither staying around the barrier regions nor inside the conductor. Finally, for the case of near resonance with a large transmission probability but $|s_{21}|^2<1$, we conclude from the above results that there is a considerable amount of charge distribution in the well region as well as on both sides beyond the double barrier. In this case the charges driven to the other side of the conductor can penetrate through the double barrier but with a small transmission probability. As a result, there is a considerable amount of charges distributed in the well region as well as beyond the double barrier. We emphasize that the fact that the charge distribution is antisymmetric is a result of overall charge conservation in the circuit. This point was also mentioned in previous works.[16,23,24]

We next consider the temperature effect on $u(x)$. First, we consider the case $a=1$, $b=2$, $\mu=0.826\,927$ (resonant) [Fig. 4(a) and 4(b)]. The curves of $u(x)$ are shown in Fig. 4(a) for various temperatures T. The $T=0$ curve is fixed at 0.5, as expected, the corresponding charge distribution is zero. As the temperature T increases, the boundary values of $u(x_L)$ and $u(x_R)$, which are given by the integral formula Eq. (6), approaches asymptotically to 1 and 0, respectively. The curves of $u(x)$ is roughly constant beyond the double barrier and they drops to 0.5 in the well region. As a result, we have a quite large amount of charge distribution around the barrier regions, but inside the well the charge distribution is still small as in the case $T=0$ [Fig. 4(b)]. The effect of temperature on $u(x)$ and $n(x)$ is clearly due to the blurred Fermi

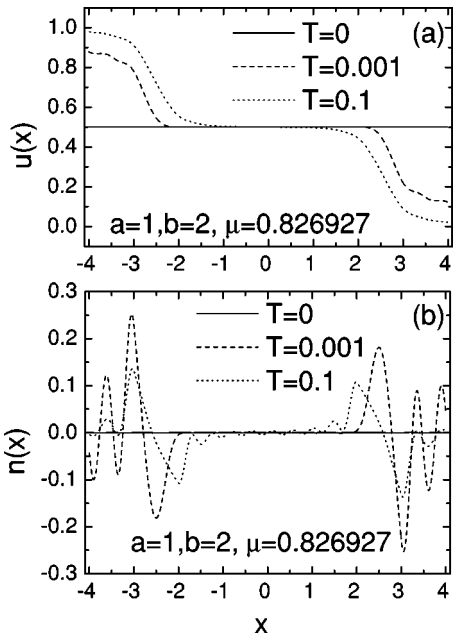

FIG. 4. The plots of internal potential (a), and charge density (b), at different temperatures for resonant case ($\mu = 0.826\,927$).

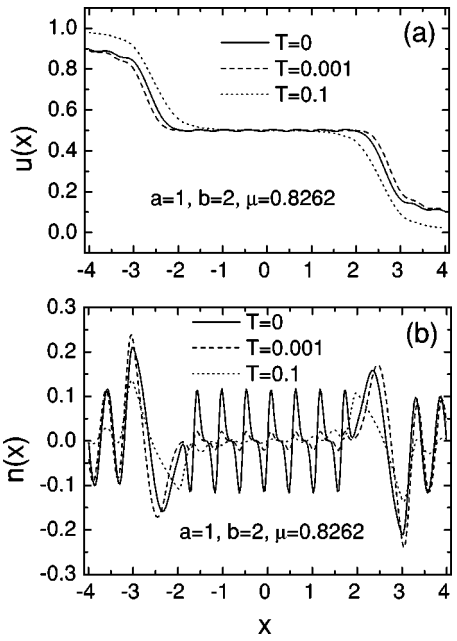

FIG. 6. The plots of internal potential (a), and charge density (b), at different temperatures for the near resonant case ($\mu = 0.8262$).

distribution at high temperature. We also consider the two nonresonant cases, $\mu = 0.8262$ and 0.7, which correspond the state of near resonance and far from resonance. For the case of near resonance, Fig. 5(a) shows that the temperature has a slight effect on $u(x)$, but Fig. 5(b) shows that it has a large effect on the charge distribution in the well. In Fig. 6, we present the results of $u(x)$ and $n(x)$ for the case far away from resonance. Furthermore, from Figs. 4–6, we can find that at high temperature the difference of the internal potential $u(x)$ and charge density $n(x)$ between the three cases become small, and it tends to vanish as the temperature increases further.

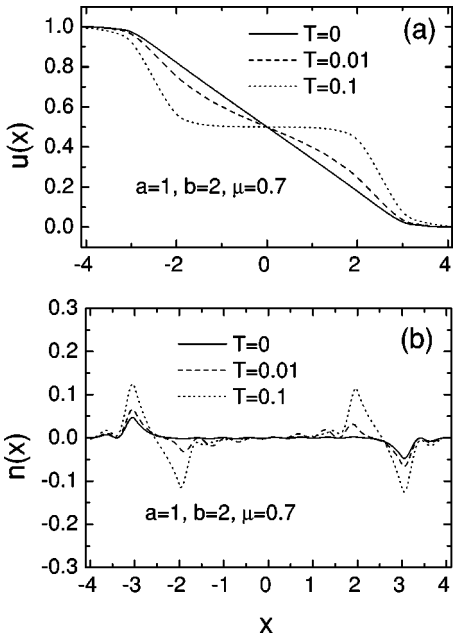

FIG. 5. The plots of internal potential (a), and charge density (b), at different temperatures for the case of far from resonance ($\mu = 0.7$).

While the distribution of internal potential and charge density reveal the information of the system under investigation, the ac conductance of the double-barrier device may provide a result that is directly capable of being verified with experimental data. We calculate the ac conductance using Eqs. (7) and (8). In Fig. 7 we present the diagonal emittance E_{11} as a function of chemical potential for $a = 1$ and $b = 2$. Figure 7(a) shows E_{11} at the neighborhood of the resonant energy $\mu = 0.826\,927$ for three temperatures $T = 0$,0.0001, and 0.001. For zero and very low temperatures, the diagonal element of the emittance is always positive (showing a capacitive behavior) when the Fermi energy μ is far from the resonant energy, but it is negative (showing an inductive behavior) when the Fermi energy is very close to the resonant energy. This is in agreement with the results obtained by Prêtre and Thomas[15] for a discrete model. Moreover, our results show that the capacitive peaks (positive maximum of E_{11}) correspond to the largest charge-density fluctuation (or charge response), and the inductive peak (negative maximum) to the resonant tunneling (zero charge fluctuation). This is in agreement with the work by Christen and Büttiker.[24] When temperature increases, both the capacitive and inductive peaks are smoothed and the amplitude of E_{11} decreases sharply with the increasing temperature, and the capacitive peaks are pushed further away from the resonance. In addition, in Fig. 7(b) and Fig. 7(c) we also present the diagonal emittance near other resonant energies for zero temperature, and find similar behavior as shown in Fig. 7(a). However, with the decrease of the resonant energies, the peaks become narrower and higher. This is due to the fact that the resonant peak of $|s_{12}|^2$ is sharper for lower resonant

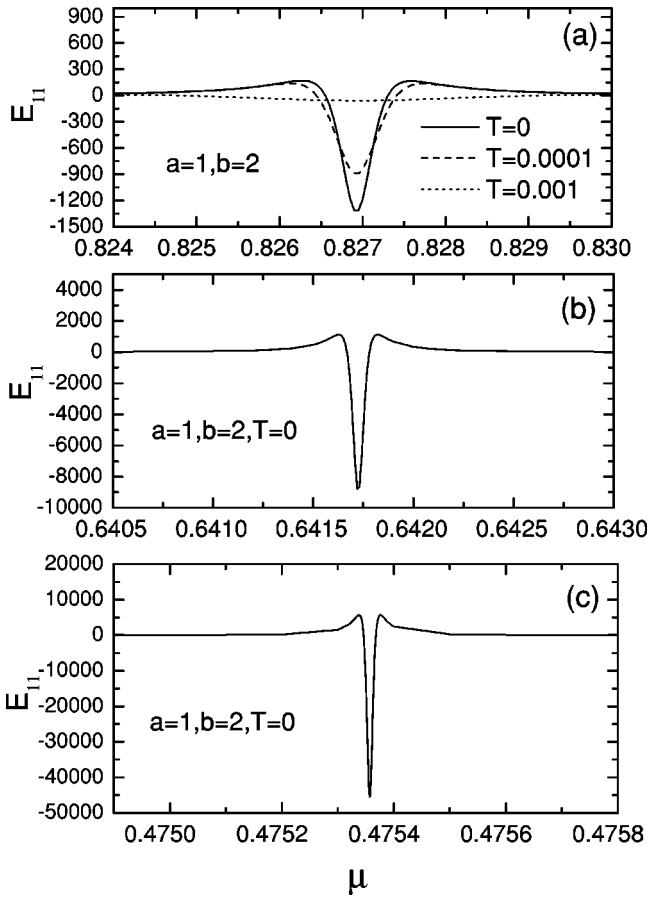

FIG. 7. The plots of the diagonal emittance element E_{11} as a function of chemical potential μ. (a) Near the resonant energy $\mu = 0.826\,927$ for different temperatures. (b) Near the resonant energy $\mu = 0.641\,724\,2$ for different temperatures for $T=0$. (c) Near the resonant energy $\mu = 0.475\,357\,0$ for different temperatures for $T=0$.

energies, which leads to sharper peaks for LPDOS $dn_{\alpha\beta}(x)/dE$. When $kT=0.001$ ($T \simeq 0.001\ V_0/k \simeq 1$ K, where $V_0 = 100$ meV) the peak structure disappears basically, and E_{11} shows a smooth dependence on μ. This effect originates from the blurred Fermi surface at finite temperature. We expect when $kT \lesssim 0.001$ the temperature T starts to play a relevant role, and above this temperature there is no significant effect of temperature on the emittance. This can also be seen clearly from Figs. 9 and 10. On the other hand, as is well known, various scattering processes with the electrons, for example, phonon scattering and defect scattering, can also suppress the resonant peaks. The authors of Refs. 8 and 25 showed that the phonon scattering had a qualitative effect on ac conductance, but at high temperature it only causes a minor modification quantitatively. So we expect that only at sufficiently low temperature those scatterings start to play an appreciable effect on the emittance, and hence the estimated temperature should be below 1 K. Above this temperature those scatterings only play a quantitatively negligible effect on the emittance.

We present the diagonal emittance E_{11} in Fig. 8 for the case of $\mu > 1$, at $T=0$ and 0.01, respectively. In this case, the

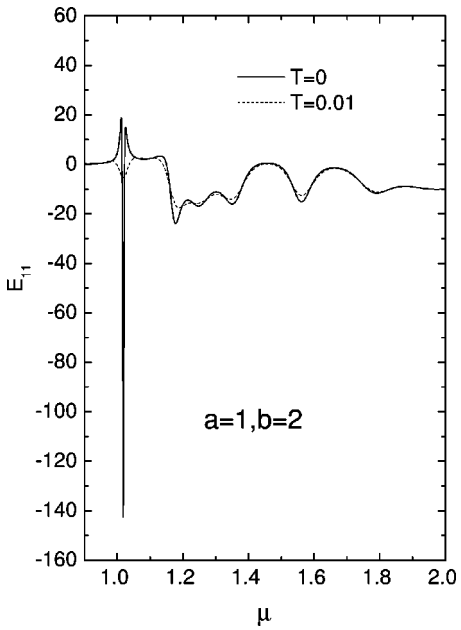

FIG. 8. The plots of the diagonal emittance element E_{11} for μ above the barriers and $T=0$ and 0.01, respectively.

Fermi energy is above the barrier height, but the emittance still fluctuates. However, the amplitude of the fluctuation and the peaks height are much smaller compared to the case of $\mu < 1$. Except around $\mu = 1$ and $\mu = 1.14$ the emittance is positive and has capacitive peaks, while it is negative elsewhere, and for very large Fermi energy it tends to zero slowly. As shown in the case of $\mu < 1$, when the temperature increases the peaks around $\mu = 1$ are suppressed greatly, but E_{11} in this region of larger μ is affected slightly.

For a better display of the temperature dependence of the emittance E_{11}, we plot E_{11} against temperature for $\mu = 0.826\,927$ (inductive peak) and $\mu = 0.826\,25$ (capacitive peak) (see Fig. 9). We see in Fig. 9(a) that the inductive peak drops very fast as temperature increases from zero, due to the blurred Fermi distribution that allowed the nonresonant cases to contribute. E_{11} drops to zero for high temperature as expected. In Fig. 9(b), we find that the capacitive peak drops very fast as temperature increases from zero and becoming an inductive peak (negative maximum) for temperature around 0.0005. This is an interesting point because the system undergoes a transition from capacitive behavior to inductive behavior as temperature grows.

Finally, we study the temperature dependence of the electrochemical capacitance C, which determines the piled-up charges for an applied ac voltage v_{ac}. Using Eq. (8), we obtain

$$C = \frac{e^2}{\sigma V_0}\int_{x_L}^{0} dx\,\frac{-d^2u(x)}{dx^2}$$

$$= \frac{e^2}{\sigma V_0}\left(\frac{du(x_L)}{dx} - \frac{du(0)}{dx}\right). \qquad (10)$$

We plot the electrochemical capacitance C against the temperature, for $m = 0.826\,927,\ 0.826\,25$. For the resonant cases

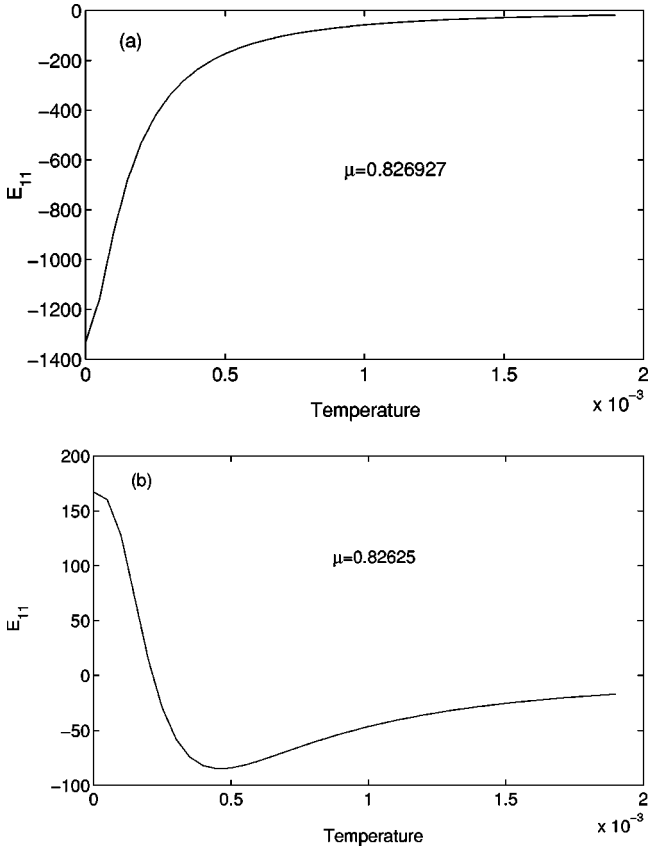

FIG. 9. The plots of the diagonal emittance element E_{11} against temperature for (a) $\mu=0.826\,927$ (inductive), and (b) $\mu=0.826\,25$ (capacitive).

[Fig. 10(a)], C is expressed in units of $e^2/(\sigma V_0)$, and it is very small at $T=0$, as has been pointed out above. As the temperature increases, C rises to a peak and then it goes off fast when the temperature increases further. The peak is obviously due to the blurred Fermi distribution function that allows the nonresonant carriers to contribute. In Fig. 10(b), $\mu=0.826\,25$ (large transmission probability but $|s_{21}|^2<1$), C is large at $T=0$. This is expected as there is a considerable amount of piled-up charges on one side of the double barrier. When T increases, the Fermi distribution is blurred and C drops very fast to small value. By comparing Figs. 9 and 10, we conclude that generally the displacement charges E_{11} and the electrochemical capacitance C are different from each other. This is similar to the case of quantum point contact discussed by Christen and Büttiker. in Ref. 24. However, positive maximum E_{11} (capacitive) corresponds to largest C, while negative maximum E_{11} (inductive) to very small C.

It should be pointed out that our calculation is only for a one-dimensional system and the charge in contacts has not been taken into consideration, and, therefore, the variation of the potential near the contacts is ignored. However, a realistic device is always connected to two- or three-dimensional contacts (electron reservoirs), and the variation of the potential near the contacts will give rise to charge distribution and accumulation. As Büttiker and Christen[26] noted, a more realistic treatment for such device may lead to a capacitive contribution.

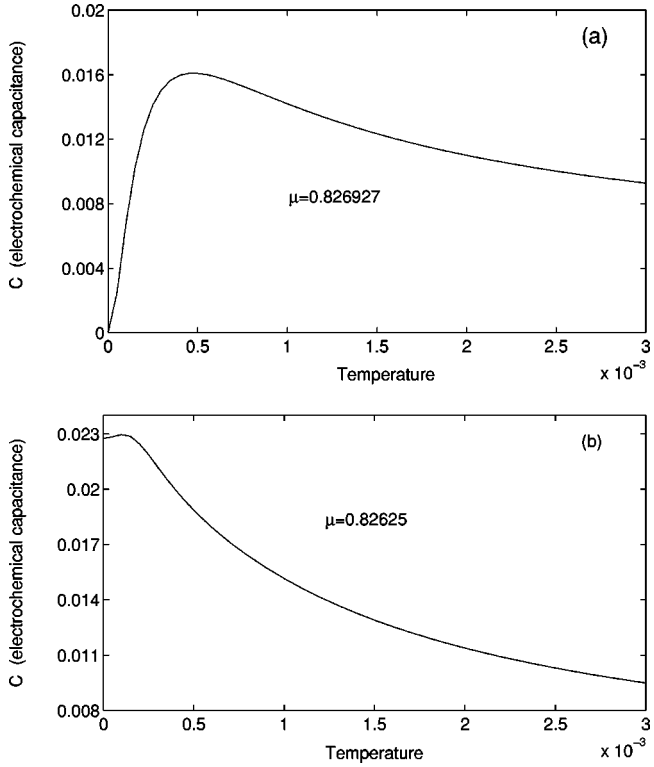

FIG. 10. The plots of electrochemical capacitance C against temperature for (a) $\mu=0.826\,27$ (inductive), and (b) $\mu=0.826\,25$ (capacitive).

IV. CONCLUSION

In conclusion, using the formalism developed by Büttiker *et al.* and within the framework of a continuous model, we have studied the dynamic response of the symmetric double-barrier resonant tunneling nanostructures, including internal potential, charge-density response and ac conductance. The results of the internal potential and the charge density show that the induced charge density has an antisymmetrical distribution profile about the well center. When the transmission probability is small (far from resonance), the antisymmetrical charge distribution exists only around the barrier regions as a response to the applied ac voltage. For the case of near resonance with a large transmission probability (but $|s_{21}|^2<1$), we find a considerable amount of charge distribution in the well region as well as on both sides beyond the double barrier. As for the resonant case or the incident energy much higher than the barrier height, our results show that the charge distribution around the double barrier is almost zero. It is found from the ac conductance that the diagonal emittance element $E_{\alpha a}$ has a crucial dependence on the Fermi level. When the Fermi energy is within the barrier height but close to the resonant energies, the emittance is negative (inductive behavior), and it reaches an inductive peak at resonant energies, while the Fermi energy is far from resonant energies, the emittance is positive (capacitive behavior) showing two capacitive peaks around both sides of the inductive peak. These results are in agreement with that in Ref. 15. In addition, we find that the capacitive peaks correspond to the maxima of charge-density fluctuation, while the induc-

tive peaks correspond to zero charge-density distribution, which agrees with the works of Christen and Büttiker.[24] We have also studied the effect of temperature on these responses, and found that the resonant effect of the system is suppressed greatly as the temperature increases and it disappears at sufficiently high temperature. So, only when the temperature is sufficient low (in our case $T=1$ K), the temperature T starts to play a relevant role. Our results also show that for the case of capacitive peaks, there is a rapid transition from capacitive to inductive behavior for the conductor as temperature increases.

Finally, we should point out that our calculation is only for a one-dimensional system, and the charge in contacts has not been taken into account in our model. However, a realistic device is always connected to two- or three-dimensional (3D) contacts (electron reservoirs), and the variation of the potential from the wires to the contacts will give rise to charge distribution in the contacts. Our calculations indicate that the strong variation of the potential corresponds to large charge fluctuation and results in large capacitive contribution to the emittance. Therefore, as Büttiker and Christen have pointed out,[26] a more realistic treatment for such device including contacts may lead to a capacitive contribution. Whereas, our results for the 1D double barrier model show that the emittance exhibits an inductive peak when the Fermi energy is in resonance, where the variation of the potential and the charge accumulation around the double barrier are almost zero. In this case, there is not any potential drop along the wires, and the potential is constant: $U(x)=\delta\mu/2$, and there is a potential drop of $\delta\mu/2$ from the two contact to the corresponding wires, resulting in the charge accumulation (in the transition region from the contacts to the wires) and a considerable capacitive contribution to the emittance. In such situation the contact effect has a considerable influence on the measurement of ac conductance. When the Fermi energy is far from resonance, our results show that the potential of the left wire is $\delta\mu$ and that of the right wire is 0, so there would be almost zero potential drop from the two contacts to corresponding wires, and the contact effect has no appreciable influence on the measurement for ac conductance. In general, for a high transmission probability of the double barrier, the potential variation near the contacts would make a considerable capacitive contribution.

ACKNOWLEDGMENTS

Xuean Zhao gratefully acknowledges support by Zhejiang Provincial Natural Science Foundation of China, Grant No. 500079; and SRF for ROCS, SEM; and Zhejiang University and College of Science for ROCS.

[1] W.R. Frensley, Superlattices Microstruct. **4**, 497 (1988).
[2] F.A. Buot and A.K. Rajagopal, Phys. Rev. B **48**, 17 217 (1993).
[3] C. Jacoboni and P.J. Price, Solid State Commun. **75**, 193 (1990).
[4] H.C. Liu, Phys. Rev. B **43**, 12 538 (1991).
[5] L.Y. Chen and C.S. Ting, Phys. Rev. Lett. **64**, 3159 (1990).
[6] Y. Fu and S.C. Dudley, Phys. Rev. Lett. **70**, 65 (1993).
[7] A.-P. Jauho, N.S. Wingreen, and Y. Meir, Phys. Rev. B **50**, 5528 (1994).
[8] M.P. Anantram and S. Datta, Phys. Rev. B **51**, 7632 (1995).
[9] T.K. Ng, Phys. Rev. Lett. **76**, 487 (1996).
[10] B. Wang, J. Wang, and H. Guo, Phys. Rev. Lett. **82**, 398 (1999).
[11] P. Nordlander, M. Pustilnik, Y. Meir, N.S. Wingreen, and D.C. Langreth, Phys. Rev. Lett. **83**, 808 (1999).
[12] T. Ivanov, Phys. Rev. B **56**, 12 339 (1997).
[13] Y. Goldin and Y. Avishai, Phys. Rev. B **61**, 16 750 (2000).
[14] Y.B. Yu, T.C. Au Yeung, W.Z. Shangguan, and K.C. Hin, Phys. Rev. B **63**, 205314 (2001).
[15] A. Prêtre and H. Thomas, Phys. Rev. B **54**, 8130 (1996).
[16] M. Büttiker, J. Phys.: Condens. Matter **5**, 9361 (1993).
[17] R. Landauer, Phys. Scr., T **42**, 110 (1992).
[18] M. Büttiker, A. Prêtre, and H. Thomas, Phys. Rev. Lett. **70**, 4114 (1993).
[19] M. Büttiker, H. Thomas, and A. Prêtre, Z. Phys. B: Condens. Matter **94**, 133 (1994).
[20] V. Gasparian, T. Christen, and M. Büttiker, Phys. Rev. A **54**, 4022 (1996).
[21] M. Büttiker, J. Math. Phys. **37**, 4793 (1996).
[22] M.P. Anantram, J. Phys.: Condens. Matter **10**, 9015 (1998).
[23] X. Zhao and Y.-X. Chen, Phys. Rev. B **64**, 085326 (2001).
[24] T. Christen and M. Büttiker, Phys. Rev. Lett. **77**, 143 (1996).
[25] T.C. Au Yeung, W.Z. Shangguan, Y.B. Yu, and K.C. Hin, Phys. Rev. B **65**, 035306 (2002).
[26] M. Büttiker and T. Christen, *Basic Elements of Electrical Conductor* in *Quantum Transport in Semiconductor Submicron Structures*, edited by B. Kramer (Kluwer Academic, Dordrecht, Massachusetts, 1996), pp. 263-291.